Biomaterials 156 (2018) 56–64

Contents lists available at ScienceDirect

Biomaterials

journal homepage: www.elsevier.com/locate/biomaterials

# A gapmer aptamer nanobiosensor for real-time monitoring of transcription and translation in single cells

Shue Wang [a, b], Yuan Xiao [b, c], Donna D. Zhang [d], Pak Kin Wong [b, c, e, *]

[a] Department of Mechanical Engineering, University of Michigan, Ann Arbor, MI 48109, USA
[b] Department of Aerospace and Mechanical Engineering, The University of Arizona, Tucson, AZ 85721, USA
[c] Department of Biomedical Engineering, The Pennsylvania State University, University Park, PA 16802, USA
[d] Department of Pharmacology and Toxicology, The University of Arizona, Tucson, AZ 85721, USA
[e] Department of Mechanical Engineering and Department of Surgery, The Pennsylvania State University, University Park, PA 16802, USA

ARTICLE INFO

*Article history:*
Received 7 June 2017
Received in revised form
23 October 2017
Accepted 21 November 2017
Available online 24 November 2017

*Keywords:*
Nanobiosensor
Gapmer
Aptamer
Locked nucleic acid
Gene expression

ABSTRACT

Transcription and translation are under tight spatiotemporal regulation among cells to coordinate multicellular organization. Methods that allow massively parallel detection of gene expression dynamics at the single cell level are required for elucidating the complex regulatory mechanisms. Here we present a multiplex nanobiosensor for real-time monitoring of protein and mRNA expression dynamics in live cells based on gapmer aptamers and complementary locked nucleic acid probes. Using the multiplex nanobiosensor, we quantified spatiotemporal dynamics of vascular endothelial growth factor A mRNA and protein expressions in single human endothelial cells during microvascular self-organization. Our results revealed distinct gene regulatory processes in the heterogeneous cell subpopulations.



## 1. Introduction

In multicellular processes such as cellular self-organization during tissue development and regeneration, cells are subjected to spatiotemporal regulation directed by cell-cell communication and environmental stimuli for forming complex tissue architectures [1]. Gene expressions in each cell are dynamically regulated throughout various synthesis and degradation pathways [2,3]. The abundances of mRNA and protein are often poorly correlated due to the diverse regulatory mechanisms, such as transcription factors, *cis*-regulatory RNA elements, post-transcriptional modifications, RNA interference, RNA binding proteins, and ubiquitination [4,5]. Effective methods for massively parallel detection of transcription and translation dynamics at the single cell level are required for defining cell states and elucidating the multicellular organization process.

Multiplex detection of mRNA and protein expression in a single cell can be performed in fixed and isolated cell samples using combinations of proximity ligation assays, RNA-seq, digital PCR, RNA in situ hybridization, and immunostaining [6–9]. Features of cell-cell coordination and dynamic regulatory schemes in multicellular processes, however, are inherently lost by study of cells in isolation and fixation. Fluorescent protein tagging systems, such as MS2 and SunTag, are available for dynamic gene expression analysis in a single cell [10,11]. These techniques have been applied for real-time observation of translation of single mRNA molecules in live cells [12–14]. Nevertheless, fluorescent protein tagging systems require genetic modifications, which are often impractical for studying endogenous molecules. Transfection of multiple reporter constructs in primary human cells with high yield is also challenging for probing multicellular processes during tissue morphogenesis and regeneration [15].

To address the need for high-throughput single cell analysis, we developed a nanobiosensor for intracellular detection of mRNA expression in live cells and tissues [16–18]. The nanobiosensor consists of locked nucleic acid (LNA) probes and gold nanorods (GNRs). The GNR spontaneously binds to the probes to form a GNR-LNA complex and effectively quenches the fluorophores conjugated to the LNA probe. The GNR also enables endocytic delivery of LNA probes into live cells without transfection or microinjection, facilitating massively parallel detection of gene expression dynamics in multicellular communities. With a target mRNA molecule, the LNA

* Corresponding author. Department of Biomedical Engineering, The Pennsylvania State University, University Park, PA 16802, USA.
*E-mail address:* pak@engr.psu.edu (P.K. Wong).

https://doi.org/10.1016/j.biomaterials.2017.11.026
0142-9612/

probe, which is the complementary sequence, is thermodynamically displaced from the GNR, allowing the fluorophores to fluoresce. The reversible binding reaction allows dynamic gene expression analysis in live cells and tissues. The nanobiosensor has been applied for investigating injury induced response in mouse cornea [17], photothermal ablation induced heat shock response in lung tissues [16], dynamic regulation of Notch1-Dll4 signaling during microvascular self-organization [18], the formation of leader cells during collective cell migration [19], and Nrf2 mediated chemoresistance in $KRAS^{G12D}$ mouse lung tumor [20]. Nonetheless, multiplex single cell detection of transcriptional and translational dynamics with high resolution during cellular self-organization remains a challenging task.

In this study, we report a multiplex nanobiosensor for monitoring mRNA and protein expression dynamics in live cells simultaneously by establishing a gapmer aptamer design along with complementary LNA probes and GNRs. The gapmer aptamer nanobiosensor is optimized for detecting intracellular protein expression and distribution with high specificity and stability in live cells. The multiplex nanobiosensor is applied to monitor vascular endothelial growth factor A (VEGF-A) mRNA and protein expressions during microvascular self-organization. The nanobiosensor simultaneously tracks the mRNA and protein expressions in hundreds of cells for over 20 h, resulting in more than 100,000 expression data points along with spatial and morphological information of individual cells in a single experiment. This technique enables us to monitor the dynamic VEGF protein and mRNA from the subcellular level to the population level. The results reveal diverse mRNA and protein expression patterns in the heterogeneous subpopulations of endothelial cells, suggesting distinct gene regulation mechanisms involved in the self-organization of the multicellular community. The capability of the nanobiosensor for massively parallel mRNA and protein detection in single live cells provides a versatile detection method for identifying functional cell subpopulations and studying the gene regulatory networks in multicellular processes.

## 2. Results

### 2.1. Intracellular protein detection with gapmer aptamer

An intracellular protein nanobiosensor was developed by incorporating molecular aptamers into the GNR-LNA nanobiosensor (Fig. 1a). Unlike previous aptamer biosensors [21–23], we designed the aptamer sequence with LNA monomers to enable intracellular protein detection with high specificity and stability. Three aptamer probe designs including DNA aptamer, gapmer aptamer, and alternating aptamer were synthesized (Fig. 1b and Supplementary Table 1) [24]. A fluorophore (6-FAM) was conjugated to the 5′ end of each aptamer probe. In this intracellular nanobiosensor, the fluorophore-labeled aptamer is displaced from the GNR and fluoresces only with the existence of a target protein. The binding affinities of the aptamer probes with GNR were characterized and optimized for VEGF protein detection (Supplementary Fig. 1a-b). Endocytic internalization of GNRs enabled delivery of the nanobiosensor into cells with high efficiency and minimal toxicity for massively parallel detection of single cells and high-resolution imaging (Fig. 1c-d) [25]. The gapmer aptamer with LNA modification in both ends of the sequence was quenched by the GNR effectively and had the highest binding affinity to VEGF protein among all aptamer probes. Consistently, the gapmer aptamer resulted in the highest contrast for high-resolution imaging in live human umbilical vein endothelial cells (HUVEC) (Supplementary Fig. 1c). The nanobiosensor was also capable of detecting autoregulation of VEGF and thrombin-induced VEGF expression in microvascular structures self-assembled on basement membrane matrix (Fig. 2 and Supplementary Fig. 2). The increase in VEGF expression was in good agreement with previous VEGF studies [26,27], supporting the applicability of the aptamer nanobiosensor for intracellular protein detection. The specificity of the gapmer aptamer was verified by VEGF knockdown with RNA interference (Supplementary Fig. 3). Since the gapmer aptamer design had the highest signal-to-noise ratio, it was utilized for detecting intracellular VEGF protein in this study.

### 2.2. Simultaneous detection of mRNA and protein in single live cells

For simultaneous detection of VEGF mRNA and protein, a complementary nucleic acid probe sequence was designed and labeled with a different fluorophore (TEX 615). The nucleic acid probe consisted of alternating LNA-DNA monomers, which were previously optimized for intracellular mRNA detection [16–18]. Both fluorophores labeled on the mRNA and protein probes were quenched due to GNR's fluorescence quenching ability. Simultaneous detection of VEGF mRNA and protein was demonstrated in HUVEC microvascular structures (Fig. 1c and Supplementary Fig. 4a). A housekeeping gene, β-actin mRNA, was also incorporated to verify the uniformity of probe delivery (Supplementary Fig. 4b). The level of β-actin expression was uniform among the cells and maintained a constant level (Supplementary Fig. 5). Unlike transfection of molecular beacons and double-stranded probes [28–30], the nanobiosensor was delivered into the cytoplasm without nuclear accumulation (Supplementary Fig. 1c). Dynamic single cell analysis of the intracellular distribution and colocalization of VEGF mRNA and protein could be performed by incorporating high-resolution imaging (Fig. 1d).

### 2.3. Intracellular imaging in heterogeneous subpopulations with distinct phenotypes

We demonstrated the capability of the multiplex nanobiosensor for probing microvascular self-organization over 20 h. This microvascular self-organization assay captures the cell migration, sprouting and elongation steps during microvascular development [31–33]. In agreement with previous studies [18,32], heterogeneous cell subpopulations with distinct morphologies and phenotypes, including aggregating cells, sprouting cells and elongating cells, were observed in the experiment (Fig. 3a). The aggregating cells assembled with other cells in the nodes and maintained low values of cell perimeter and area. The sprouting cells, which connected to other cells on one end, displayed steady increases in cell perimeter and area. In contrast, the elongating cells, which connected to neighboring cells on both ends, displayed rapid increases in cell perimeter and area during microvascular self-organization. Similar microvascular networks were observed with and without the nanobiosensors (Supplementary Fig. 2). This observation suggests the nanobiosensor does not significantly interfere with the microvascular self-organization process.

We incorporate high-resolution imaging to investigate the spatial distribution and colocalization of VEGF mRNA and protein in these cell subpopulations during microvascular network formation (Fig. 3b-d). Overall, the gene expression distributions in endothelial cells were non-uniform and displayed distinct signatures among the cell subpopulations. Transient “hotspots” of VEGF mRNA and protein colocalization were observed in cells. In aggregating cells, the colocalization hotspots were observed throughout the experiment. This observation was supported quantitatively by analyzing the pixel values above the threshold (Supplementary Fig. 6). The Pearson's correlation coefficient of aggregating cells maintained a

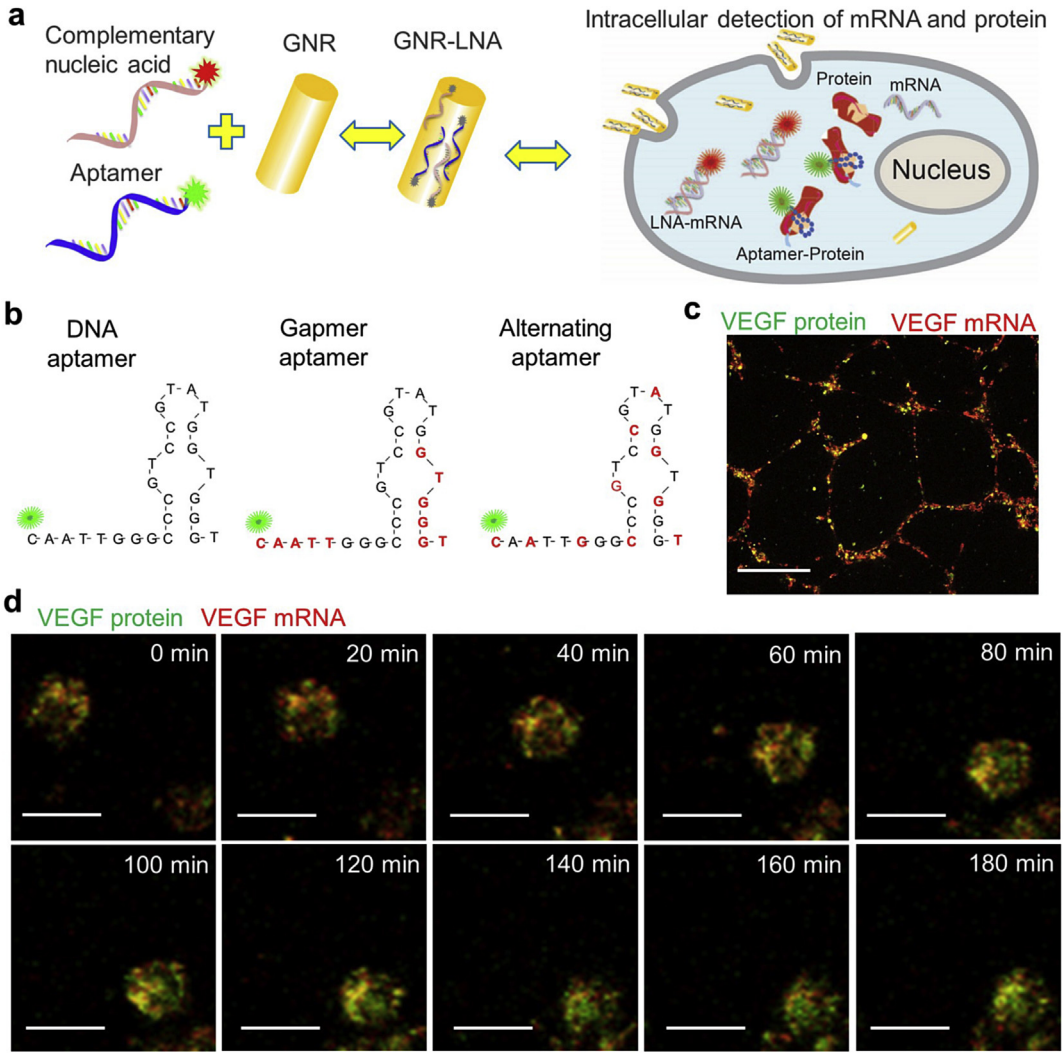


**Fig. 1. A multiplex nanobiosensor for simultaneous detection of mRNA and protein in single cells during multicellular organization**. (a) Schematic illustration of the multiplex nanobiosensor. The nucleic acid probes spontaneously bind to the gold nanorods, which quench the fluorophores conjugated on the probes. The gold nanorods facilitate internalization of the multiplex nanobiosensor for intracellular detection. (b) Three designs of the protein nanobiosensor with DNA aptamer, gapmer aptamer, and alternating aptamer. LNA monomers are highlighted in red. A fluorophore (6-FAM) is conjugated at the 5′ end of the aptamer sequence. (c) Multiplex detection of VEGF mRNA and protein in HUVEC microvascular structures. Scale bar, 200 μm. (d) Dynamic tracking of intracellular VEGF mRNA (red) and protein (green) in a single HUVEC cell. Scale bars, 10 μm. Images are representative of five independent experiments. (For interpretation of the references to colour in this figure legend, the reader is referred to the web version of this article.)

high value (over 0.9) throughout the experiment. Sprouting cells also displayed a high level of VEGF mRNA and protein colocalization initially (correlation coefficient over 0.9). The correlation coefficient decreased and maintained an intermediate level (correlation coefficient between 0.7 and 0.8) after the first hour of microvascular self-organization (Supplementary Fig. 7). In contrast, elongating cells displayed transient dynamics of colocalization hotspots in the experiment. Colocalization hotspots were mainly observed at the beginning of the experiment. The correlation coefficient decayed rapidly in the first hour and fluctuated at a low level of mRNA and protein colocalization (correlation coefficient between 0.5 and 0.7) compared to sprouting and aggregating cells. These observations suggest the heterogeneous subpopulations have distinct expression patterns.

### *2.4. Dynamic gene expression profiling of VEGF mRNA and protein in single cells*

The nanobiosensor allows dynamic monitoring of the VEGF mRNA and protein expression levels at the single cell level. We, therefore, investigated the VEGF mRNA and protein dynamics in individual cells during the early stage of microvascular self-organization. In general, the mRNA and protein expression levels are the results of transcription, mRNA degradation, translation, and protein degradation. Close examination of mRNA and protein expression dynamics reveals diverse gene expression behaviors for the cell subpopulations. Fig. 4 shows the expression profiles of representative cells of each subpopulation. For aggregating cells (Fig. 4a, cells 1–3), the levels of VEGF mRNA were approximately constant and the protein levels increased monotonically. As demonstrated by a computational model of expression kinetics (Supplementary Fig. 9-10), this behavior is anticipated when the translational rate is constant.

Interestingly, transcriptional control was observed in other cell subpopulations. For instance, sprouting cells displayed a transient increase in VEGF mRNA and gradually decreased after the first hour (e.g., cells 4–5). The decrease in VEGF mRNA could be a result of a reduction of transcription rate or an increase in mRNA degradation rate. A longer duration of VEGF mRNA increase was also observed in some cells (e.g., cell 6). Despite the heterogeneous expression

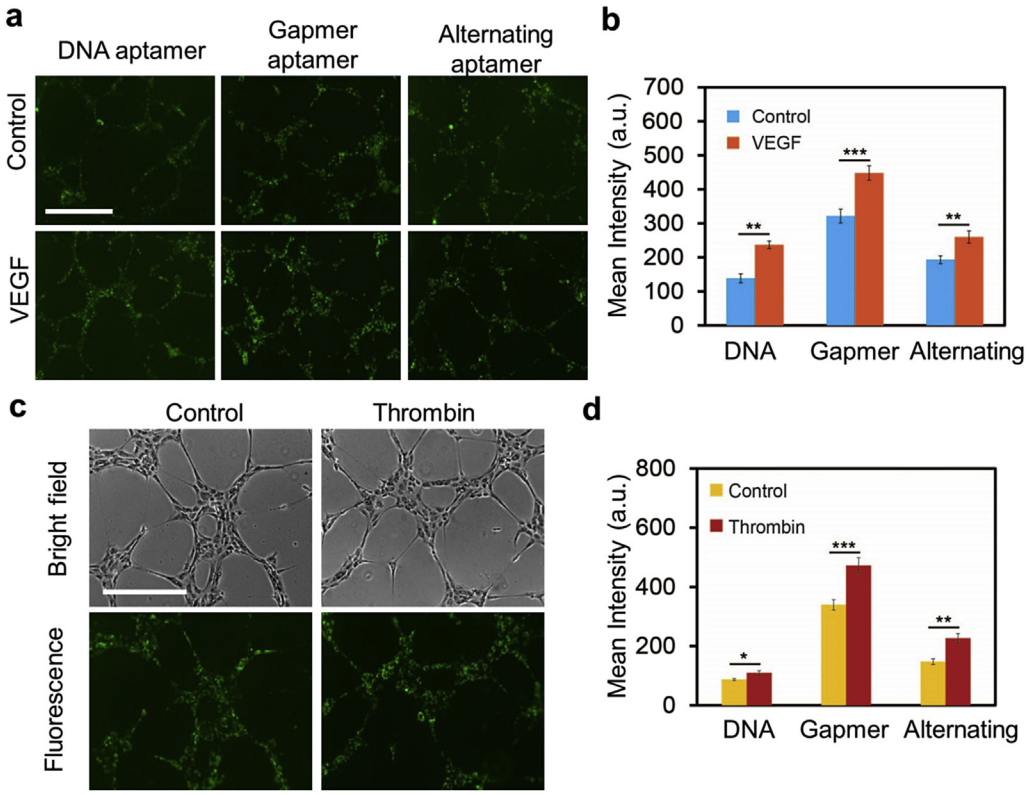


**Fig. 2. Optimization of aptamer probe designs for intracellular VEGF protein detection in HUVEC microvascular structures.** (a) Fluorescence images characterizing VEGF protein detection with and without VEGF treatment using DNA aptamer, gapmer aptamer and alternating aptamer. Human recombinant $VEGF_{165}$ (25 ng/ml) were added after cell seeding. Fluorescence images were taken after 6 h of incubation. Scale bar: 200 μm. (b) Comparison of VEGF protein detection using the aptamer probes in HUVEC microvascular structures. Data are expressed as mean ± s.e.m. (n = 3; **P < 0.01 and ***P < 0.001; unpaired Student's t-test). (c) Thrombin induced VEGF protein expression in HUVEC microvascular structures. Bright field and fluorescence images of microvascular structures with and without thrombin (buffer). Human α-thrombin (1 IU/ml) were added immediately after cell seeding. Images were acquired after 6 h of incubation. Fluorescence images illustrating VEGF protein detection using the gapmer aptamer nanobiosensor. Scale bar: 200 μm. (d) Comparison of three aptamer probes for VEGF protein detection in microvascular structures with and without thrombin treatment. Data are expressed as mean ± s.e.m. (n = 3; *P < 0.05, **P < 0.01, ***P < 0.001; unpaired Student's t-test).

dynamics, the VEGF protein expressions generally followed the expression dynamics of VEGF mRNA for the majority of cells. A delay of the protein dynamics, which was presumably due to the time scales of translation and maturation of VEGF protein, was observed in the cells. This observation suggests that gene expression dynamics were primarily controlled at the transcription level in these cells. For elongating cells (cells 7–9), the level of VEGF mRNA increased initially and gradually decreased after a short duration, similar to sprouting cells. The duration ranged from 30 min to over 120 min, resulting in more diverse expression profiles for elongating cells. Interestingly, a large variation of VEGF protein dynamics relative to the VEGF mRNA was also observed for elongating cells. In particular, a reduction in VEGF mRNA expression level did not always result in a decrease in VEGF protein. Since the VEGF protein level is the combined result of translation and degradation, the results suggested additional mechanisms of translational control of VEGF expression, such as modification of the VEGF degradation pathway (e.g., proteases), are involved in elongating cells.

### 2.5. Correlation of mRNA and protein levels at the population scale

The multiplex nanobiosensor is capable of detecting VEGF protein and mRNA expressions in a large number of cells simultaneously. By developing a custom-design image analysis program, we studied the correlation of mRNA and protein expressions at the population scale (Fig. 5a and Supplementary Fig. 11). The correlation between mRNA and protein expression levels were determined at different time points. The data revealed significant deviations between mRNA and protein expressions at the beginning of the experiment. The correlation coefficients $R^2$ fluctuated between 0.792 and 0.845 in the first hour. The computational model was also applied to predict the correlations between mRNA and protein expressions using the experimental data at 5 min as the initial condition (Fig. 5b). The computational model correctly predicted similar values of correlation coefficients (from 0.767 to 0.8621) at the early stage of microvascular self-organization. We then studied the correlation between mRNA and protein expressions between 1 and 12 h during microvascular self-organization using the multiplex nanobiosensor and computational model (Fig. 5). The correlation coefficient increased gradually between 1 and 12 h from 0.8330 to 0.9251. In agreement, the computational model predicted an increasing trend of the correlation coefficient. The values increased from 0.8256 to 0.9972. These results collectively suggest that initial expression levels as well as the kinetics in protein translation and maturation had significant effects on the correlation between VEGF protein and mRNA, providing a possible explanation for the low level of correlation at the beginning of the experiment. For a time scale compatible with protein expression and maturation (e.g., 1–12 h), the initial randomness of the expression levels had a much smaller influence on the correlation between mRNA and protein expressions.

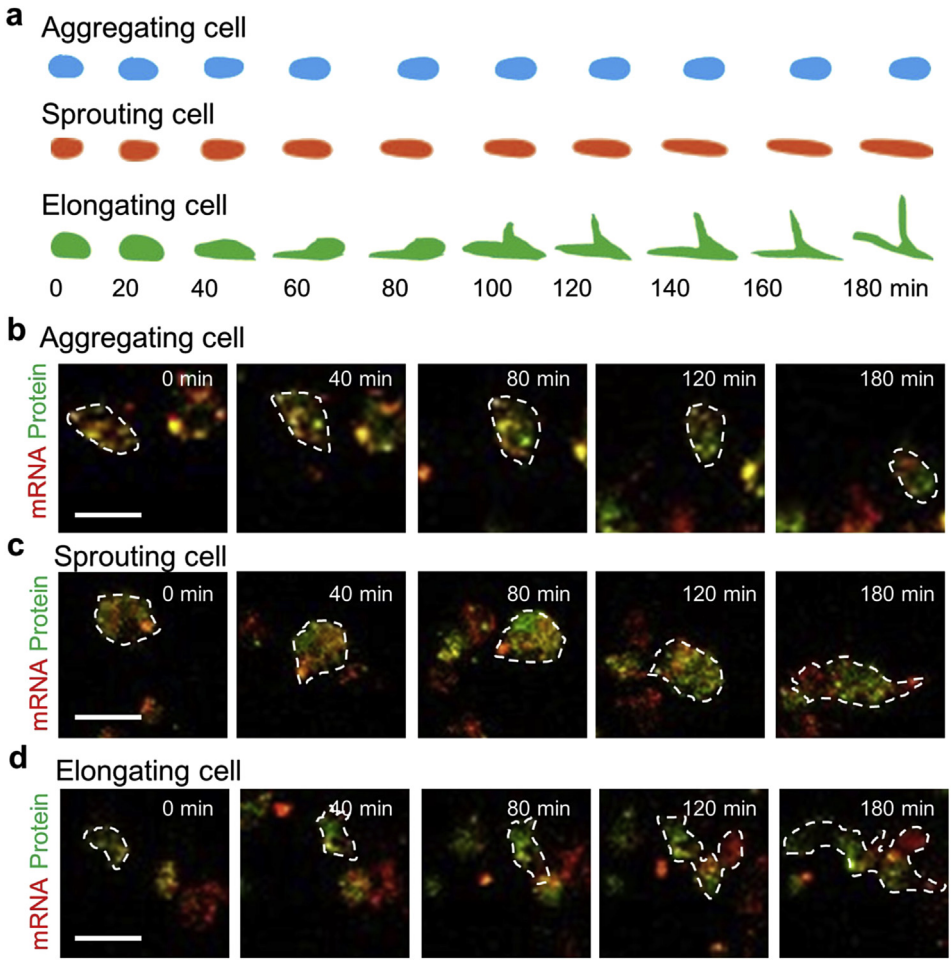


**Fig. 3. Cell subpopulations displayed distinct morphological patterns and intracellular gene expression patterns during microvascular self-organization.** (a) Morphologies of three distinctive cell subpopulations observed during microvascular self-organization. (b–d) Aggregating cells, sprouting cells and elongating cells displayed diverse expression levels and distributions of VEGF mRNA and protein during microvascular self-organization. White dotted lines indicate the cell boundaries. Scale bars, 20 μm. Images are representative of five independent experiments.

## 3. Discussion

In this study, a multiplex nanobiosensor is developed for monitoring intracellular mRNA and protein expression dynamics in live cells. By incorporating LNA monomers in the aptamer sequence, we circumvented the stability issue of aptamers for intracellular protein detection. Using VEGF autoregulation, thrombin stimulation, and siRNA knockdown, the binding affinity, signal-to-noise ratio and stability of the aptamer designs were characterized and optimized for intracellular VEGF detection in HUVEC cells. The gapmer aptamer probe with LNA monomers in both ends of the sequence possessed the best signal-to-noise ratio and performance for intracellular protein detection. This gapmer strategy can be applied, in principle, when a DNA or RNA aptamer is available. Otherwise, affinity-based selection and optimize will be required to identify an aptamer. By incorporating the gapmer aptamer for protein detection along with an alternating LNA/DNA probe for mRNA detection, a multiplex nanobiosensor was established for investigating VEGF expression dynamics. This multiplex nanobiosensor was capable of detecting multiple genes, such as VEGF mRNA, VEGF protein, and β-actin mRNA, in the same cell. We applied the multiplex nanobiosensor to monitor VEGF mRNA and protein expression dynamics during microvascular self-organization. The expression dynamics of VEGF mRNA and protein at the subcellular, single cell and population levels were monitored during microvascular self-organization.

Multiplex detection at both transcriptional and translational levels in live cells has been a challenging task. Despite the recent development in single cell analysis, there is a lack of effective approaches for simultaneous monitoring of mRNA and protein in the same cell dynamically [34]. Current methods of single cell analysis typically do not allow multiplex detection and are often limited to a specific time point due to the requirement of cell fixation or lysis [6–9]. Fluorescent protein tagging systems represent a powerful platform for live cell imaging [10,11]. Real-time imaging of translation on single mRNA transcripts in live cells was demonstrated for studying intracellular dynamics of protein synthesis, transport, and localization [12–14]. Multiplex detection of a large number of cells with fluorescent protein tagging systems, however, can be hindered by the requirement of genetic modifications, the availability of high-affinity binding motifs, and the efficiency of transfecting multiple reporter transcripts in the same cells [15]. These issues are particularly challenging for delicate primary human cells. On the other hand, our approach provides an effective method for monitoring the gene expression dynamics during multicellular processes. The multiplex nanobiosensor allows not only high-resolution imaging of gene expression dynamics but also massively parallel detection of mRNA and protein dynamics for a

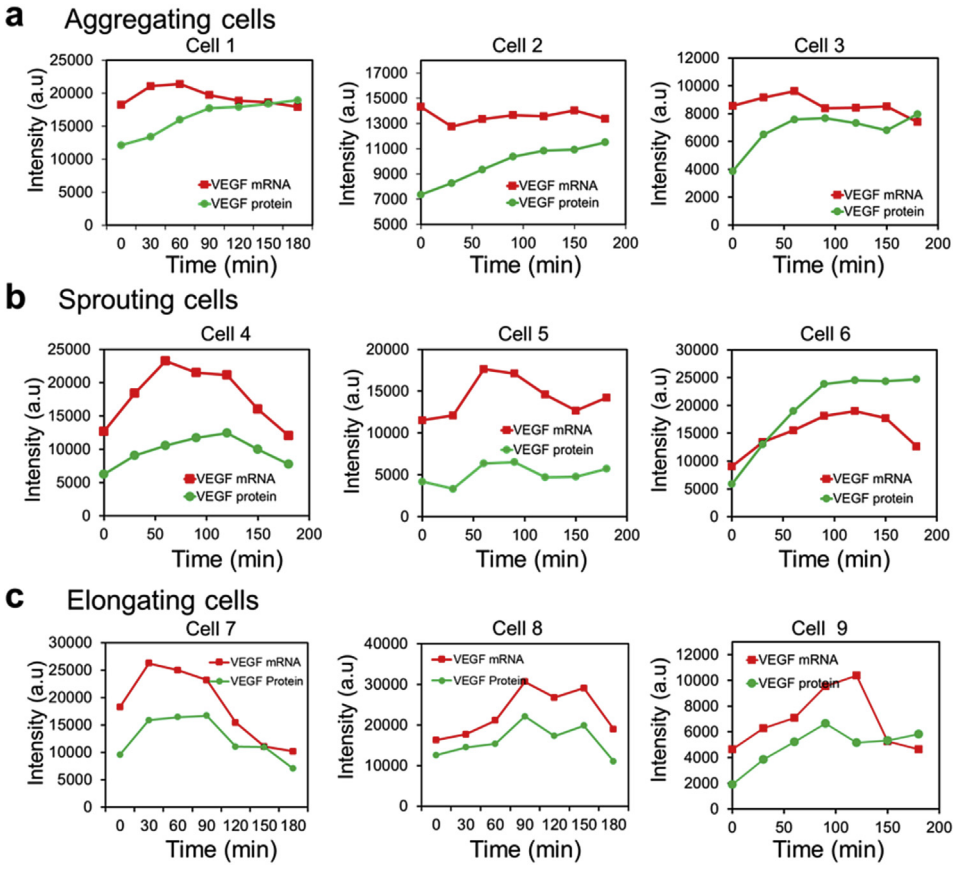


**Fig. 4. Dynamics of mRNA and protein expressions in representative cells during microvascular self-organization.** (a–c) VEGF mRNA and protein expression dynamics in cells that are representative of (a) aggregating cell, (b) sprouting cell, and (c) elongating cell subpopulations. Aggregating cells maintained a constant level of VEGF mRNA and a monotonic increase of VEGF protein. Sprouting cells and elongating cells displayed transient increases in VEGF expressions. Data are representative of over 1200 cells.

large number of cells. This technology may also open new opportunities for detecting disease biomarkers and characterizing rare cell populations, e.g. cancer stem cells and circulating tumor cells, in clinical samples. Further research will be required to translate the single cell analysis technology to monitor disease progression, measure therapeutic responses, and predict the clinical outcome.

The multiplex nanobiosensor revealed unexpected gene regulatory mechanisms in the cell subpopulations during microvascular self-organization. Autonomous organization of angioblasts and vascular progenitors with distinct phenotypic behaviors was observed during microvascular development for decades [35]. Nevertheless, the molecular processes driving the distinct phenotypes during the self-organization process remained elusive. We addressed these fundamental questions by performing dynamic gene expression analysis along with phenotypic characterization of human endothelial cells. As indicated by colocalization hotspots inside the cells, single cell expression dynamics, and correlation analysis at the population level, VEGF was highly dynamic during the early stage of the microvascular self-organization process. The combination of experimental and computational analyses suggest that VEGF expressions were controlled at multiple levels and depended on the subpopulations. Aggregating cells maintained a relatively constant level of VEGF mRNA and expressed VEGF protein continuously in the early stage of the process. This observation is in good agreement with the suggested roles of aggregating cells in attracting cells at the centers of the autocrine gradients during microvascular self-organization [33]. On the other hand, sprouting and elongating cells displayed transient expression dynamics controlled at both transcriptional and translational levels, as indicated by single cell expression dynamics and intracellular gene expression patterns. The single cell dynamic data along with the computational model also shed light on the apparent discrepancy of the mRNA and protein expressions at the beginning of the process. The expression kinetics of transient genes and initial randomness in the expression level may potentially explain the poor correlation of mRNA and protein in other studies. Collectively, our results suggest areas of systematic investigation of the mechanisms of transcriptional and translational control and underscore the significance of dynamic multiplex detection of single cells for investigating complex multicellular processes.

## 4. Materials and methods

### 4.1. Multiplex nanobiosensor design

The multiplex nanobiosensor consists of GNR, mRNA probes, and aptamer probes. The mRNA probe is a single-stranded 20-base nucleotide sequence with alternating LNA/DNA monomers. The mRNA probe was labeled with a fluorophore (TEX615) at the 5′ end for mRNA detection. The design procedure of mRNA probe was reported previously [36]. Briefly, the LNA probe was designed to be complementary to a loop region of the target mRNA structure. The secondary structures, binding affinity, and specificity were optimized using the mFold server and NCBI Basic Local Alignment Search Tool (BLAST) database. The aptamers are nucleic acid sequences identified using an iterative enrichment technique. Oligos with high affinity and specificity to the target protein or cell are isolated from a large random sequence pool with multiple rounds

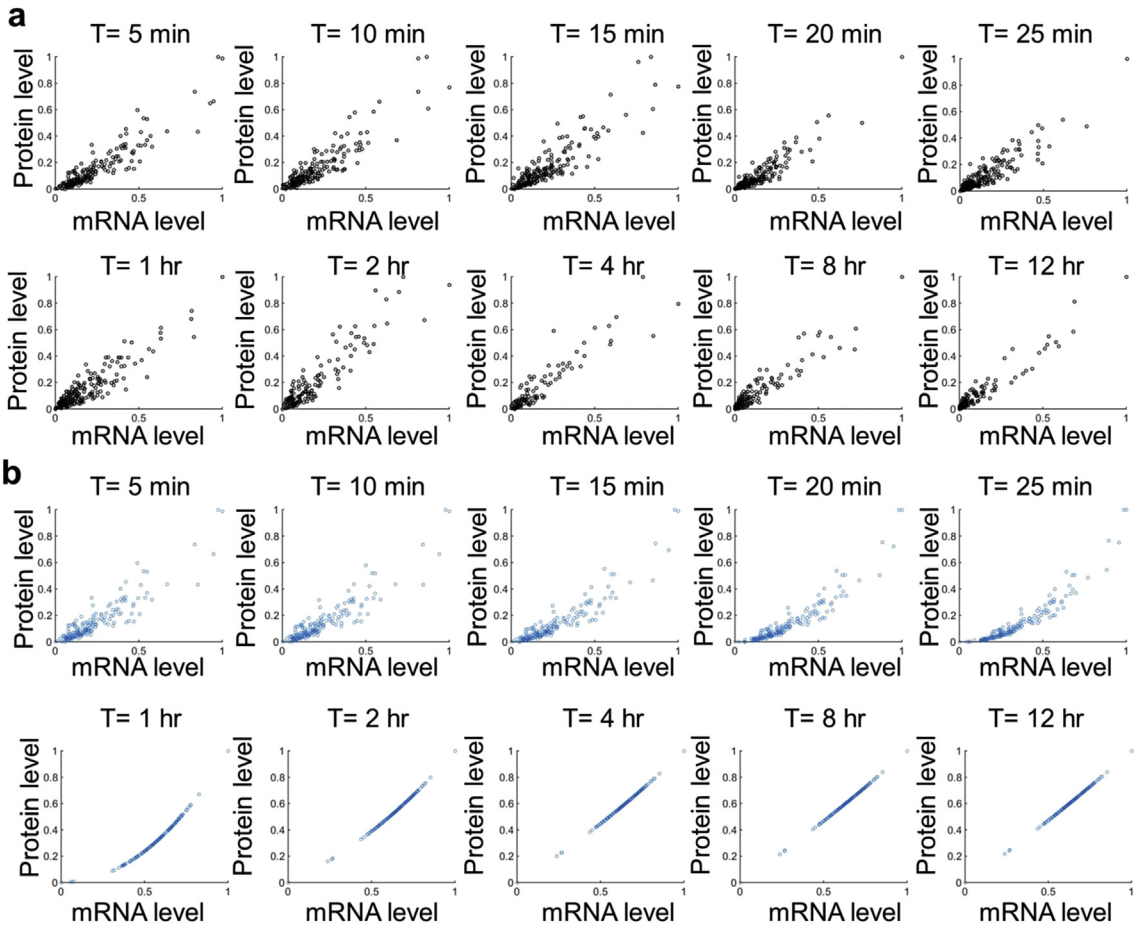


**Fig. 5. Correlation between mRNA and protein expressions at the population level during microvascular self-organization**. (a) Correlation of experimentally measured mRNA and protein expressions at different time points. The mRNA and protein levels were determined by the fluorescence intensity. The intensity values were normalized between 0 and 1 for comparison. The correlation coefficients were 0.8446, 0.8125, 0.7916, 0.8424, 0.8212, 0.833, 0.8552, 0.8612, 0.8827, and 0.9251, respectively. (b) The correlation between mRNA and protein levels using the computational model. The initial conditions were acquired from experimental results. The correlation coefficients were 0.8325, 0.8405, 0.8621, 0.8073, 0.767, 0.8256, 0.9203, 0.9874, 0.995, and 0.9972 respectively.

of selection. For instance, Systematic Evolution of Ligands by Exponential Enrichment (SELEX) is one of the iterative enrichment methods used to identify aptamers [37]. In our study, the aptamer sequence (5′-3′, CAATTGGGCCCGTCCGTATGGTGGGT) for VEGF protein detection was acquired from the literature [24]. Three protein probes, DNA probe, gapmer probe, and alternating probe, were designed by adjusting the number and location of LNA monomers (Supplementary Table 1). To characterize the uniformity of probe loading, three different probes, VEGF mRNA, VEGF protein and β-actin mRNA, were designed with different fluorophores (Supplementary Table 2). To minimize fluorescence bleed-through between fluorophores, two fluorophores that are further apart (6-FAM and TEX 615) were utilized to detect VEGF protein and mRNA (Supplementary Table 3). The gapmer aptamer probe was labeled with a fluorophore (6-FAM) at the 5′ end for VEGF protein detection, the alternating LNA/DNA probe was labeled with a fluorophore (TEX 615) for VEGF mRNA detection (Supplementary Table 3). A β-actin mRNA probe was designed as a control. All LNA probes and corresponding target DNA sequences for calibration were synthesized by Exiqon Inc.

### 4.2. Preparation of multiplex nanobiosensor

GNRs with 10 nm axial diameter and 67 nm length were acquired from Nanopartz, Inc. GNRs were modified with MUTAB with positive surface charge. All the probes (aptamer probes and mRNA probes) were prepared in 1× Tris–EDTA buffer at a concentration of 100 nM. The probes were incubated at 95 °C for 5 min in a water bath and cooled down to 70 °C over the course of 1 h. GNRs were incubated with the probes at 70 °C for 30 min and cooled down to room temperature slowly. The GNR probes were then incubated with cells at a concentration of $2 \times 10^{11}$ particles/ml for 4 h for cellular uptake when the cells reached about 80% confluency.

### 4.3. Cell culture and reagents

Human umbilical vein endothelial cells (HUVECs, Lonza) were cultured in EBM-2 medium (endothelial growth basal medium, Lonza) and supplemented with 2% fetal bovine serum (FBS), 0.1% human epidermal growth factor, 0.1% R3-insulin-like growth factor-1, 0.1% ascorbic acid, 0.04% hydrocortisone, 0.4% human fibroblast growth factor β, 0.1% heparin, and 0.1% gentamicin/amphotericin B. The cells were cultured in an incubator at 37 °C with 5% CO [2] with medium change every two days. The cells were washed using 1× PBS and harvested using 0.25% Trypsin-EDTA (Invitrogen) when the cells became confluent. HUVECs from passage 2–7 were used in the experiments. For siRNA experiments, HUVECs were seeded at a density of $1 \times 10^5$ cells/mL with a volume of 2 mL in 6-well plate, and cultured overnight. The cells were then transfected with 20 nM siRNA from Qiagen (Valencia, CA, USA)

using the Lipofectamine LTX Reagent (Fisher Scientific), following the manufacturer's instructions, and incubated for 48 h. Cells were then incubated with the multiplex nanobiosensor for endocytic uptake. Cells were imaged after 4 h of incubation.

### 4.4. In vitro microvascular organization

Growth factor reduced Matrigel (Corning® Matrigel® Matrix) was thawed overnight on ice and added to glass-bottom 24-well plates (MatTek Corporation). After 30 min incubation at 37 °C for gelation, HUVECs were seeded onto the solidified gel at a density of 250 cell/mm$^2$. The 24-well plate was placed in a microscope incubator (Okolab) equipped for live-cell imaging. Spatiotemporal mRNA and protein expression dynamics were then monitored during microvascular self-organization.

### 4.5. Imaging and data analysis

For VEGF protein detection, bright-field and fluorescence images were captured using an inverted microscope (Nikon, TE2000-U) with an HQ2 CCD camera (SensiCamQE, Cook Cork.). All fluorescence images of endothelial cells were taken with the same settings with a 1 s exposure time for comparison. For simultaneous detection of VEGF mRNA and protein expression dynamics, time-lapse microscopy of microvascular self-organization was performed using a confocal single molecule detection platform (Leica TCS SP8) with an interval of 5 min. The Z-stack images were acquired with an optical slice thickness of 1 μm and separate exposures of two different channels (6-FAM, excitation: 488 nm, emission: 535 nm; TEX 615, excitation: 591 nm, emission: 613 nm). Experiments were repeated independently at least three times. Data collection and imaging analysis were performed using Leica Application Suit and Matlab. The mRNA and protein levels were quantified by measuring the fluorescence intensity. A custom-design Matlab image processing program was used to quantify single cell intensity at different channels. Briefly, the original images were converted to grayscale intensity images. A flat, disk-shaped structural element was created and morphological operations were applied to remove the background noise. Cell segmentation was then performed using an adaptive threshold. The intensities of each cell at different channels were then calculated individually. The scatterplot and histogram of VEGF mRNA and protein expression were generated accordingly.

### 4.6. Western blot

Cell lysates were collected in radioimmunoprecipitation buffer (RIPA buffer). Samples were subjected to 12% SDS-PAGE followed by transfer to PVDF membranes. Blotted membranes were incubated with rabbit anti-VEGF primary antibodies (Santa Cruz Biotechnologies, Santa Cruz, CA, USA) in blocking buffer overnight at 4 °C, followed by incubation with alkaline-phosphatase-conjugated secondary antibodies (Sigma-Aldrich, St. Louis, MO, USA) for 1 h at room temperature. The blots were resolved using Western blue stabilized substrate (Promega, Madison, WI, USA).

### 4.7. Computational model of gene expression dynamics

A computational model was developed to study the dynamics of mRNA and protein expressions. In this model, the mRNA is synthesized at a rate of $k_m$ and degraded at a rate of $d_m$. The protein synthesis process has two steps. The mRNAs are first translated into immature protein at a rate of $k_p$ and degraded at a rate of $d_p$. The immature protein will then fold and form mature functional protein at a rate of $k_{mp}$. The mature protein is degraded at a rate of $d_{mp}$. The kinetics of the synthesis process of mRNA and protein can be described by the following differential equations (1)–(3).

$$\frac{dm}{dt} = k_m - d_m \cdot [m] \tag{1}$$

$$\frac{dp}{dt} = k_p \cdot [m] - k_{mp} \cdot [p] - d_p \cdot [p] \tag{2}$$

$$\frac{dp_m}{dt} = k_{mp} \cdot [p] - d_{mp} \cdot [p_m] \tag{3}$$

Here, $dm/dt$, $dp/dt$, and $d_{pm}/dt$ are the rates of change of mRNA [$m$], immature protein [$p$], and mature protein [$p_m$]. $k_m$, $k_p$ and $k_{mp}$ are the first order transcription rate, translation rate and protein maturation rate, respectively. $d_m$, $d_p$, and $d_{mp}$ are the mRNA, immature protein, and mature protein first order degradation rates. The mRNA degradation rate is inversely to the mRNA half-life $\tau_m$, $d_m = \ln(2)/\tau_m$. The protein degradation rate is the inverse of protein half-life, $d_p = \ln(2)/\tau_p$. As indicated in equation (1), the mRNA level [$m$], depends on the transcription rate and the mRNA half-life. The protein level depends on the number of mRNAs, translational rate, and protein half-life. This model can be solved analytically. The mRNA half-life and protein half-life can be acquired according to previous literature [38–40]. The transcription rate and translation rate were determined based on the experimental data. First, the mRNA and protein levels were quantified by measuring average fluorescence intensity using the nanobiosensor and calibration. A measurement of the relative amount of labeled mRNAs and proteins over time revealed the time scale of mRNA synthesis and protein synthesis. The simulation curves were then fitted by adjusting the transcription rate $k_m$ and translation rate $k_p$. All the numbers were normalized from 0 to 1 for comparison. The reaction rates were assumed to be constant for studying the effect of transcriptional and translational control on the mRNA and protein expression levels.

### 4.8. Statistical analysis

Data are presented as mean ± s.e.m. Experiments were conducted in triplicate, and repeated at least three independent times. Student's t-tests were performed to analyze statistical significance between experimental groups. For comparing multiple groups, a one-way analysis of variance and Tukey's post hoc test were used. Statistically significant P values were assigned as follows: *, $P < 0.05$; **, $P < 0.01$ or ***, $P < 0.001$.

## Conflicts of interest

The authors declare no competing financial interests.

## Acknowledgments

This work was supported by National Institutes of Health Director's New Innovator Award (DP2OD007161).

## Appendix A. Supplementary data

Supplementary data related to this article can be found at https://doi.org/10.1016/j.biomaterials.2017.11.026.

## References

[1] E. Karsenti, Self-organization in cell biology: a brief history, Nat. Rev. Mol. Cell Biol. 9 (3) (2008) 255–262.
[2] B. Jones, Gene expression: layers of gene regulation, Nat. Rev. Genet. 16 (3) (2015) 128–129.

[3] T.I. Lee, R.A. Young, Transcriptional regulation and its misregulation in disease, Cell 152 (6) (2013) 1237–1251.
[4] L. Peshkin, M. Wuhr, E. Pearl, W. Haas, R.M. Freeman Jr., J.C. Gerhart, A.M. Klein, M. Horb, S.P. Gygi, M.W. Kirschner, On the relationship of protein and mRNA dynamics in vertebrate embryonic development, Dev. Cell 35 (3) (2015) 383–394.
[5] T. Maier, M. Guell, L. Serrano, Correlation of mRNA and protein in complex biological samples, FEBS Lett. 583 (24) (2009) 3966–3973.
[6] S. Darmanis, C.J. Gallant, V.D. Marinescu, M. Niklasson, A. Segerman, G. Flamourakis, S. Fredriksson, E. Assarsson, M. Lundberg, S. Nelander, B. Westermark, U. Landegren, Simultaneous multiplexed measurement of RNA and proteins in single cells, Cell Rep. 14 (2) (2016) 380–389.
[7] A.P. Frei, F.A. Bava, E.R. Zunder, E.W. Hsieh, S.Y. Chen, G.P. Nolan, P.F. Gherardini, Highly multiplexed simultaneous detection of RNAs and proteins in single cells, Nat. Methods 13 (3) (2016) 269–275.
[8] C. Albayrak, C.A. Jordi, C. Zechner, J. Lin, C.A. Bichsel, M. Khammash, S. Tay, Digital quantification of proteins and mRNA in single mammalian cells, Mol. Cell 61 (6) (2016) 914–924.
[9] J. Kochan, M. Wawro, A. Kasza, Simultaneous detection of mRNA and protein in single cells using immunofluorescence-combined single-molecule RNA FISH, BioTechniques 59 (4) (2015), 209–12, 214, 216 passim.
[10] M.E. Tanenbaum, L.A. Gilbert, L.S. Qi, J.S. Weissman, R.D. Vale, A protein-tagging system for signal amplification in gene expression and fluorescence imaging, Cell 159 (3) (2014) 635–646.
[11] A.R. Buxbaum, G. Haimovich, R.H. Singer, In the right place at the right time: visualizing and understanding mRNA localization, Nat. Rev. Mol. Cell Biol. 16 (2) (2015) 95–109.
[12] B. Wu, C. Eliscovich, Y.J. Yoon, R.H. Singer, Translation dynamics of single mRNAs in live cells and neurons, Science 352 (6292) (2016) 1430–1435.
[13] X. Yan, T.A. Hoek, R.D. Vale, M.E. Tanenbaum, Dynamics of translation of single mRNA molecules in vivo, Cell 165 (4) (2016) 976–989.
[14] C. Wang, B. Han, R. Zhou, X. Zhuang, Real-time imaging of translation on single mRNA transcripts in live cells, Cell 165 (4) (2016) 990–1001.
[15] S. Tyagi, Imaging intracellular RNA distribution and dynamics in living cells, Nat. Methods 6 (5) (2009) 331–338.
[16] R. Riahi, S. Wang, M. Long, N. Li, P.Y. Chiou, D.D. Zhang, P.K. Wong, Mapping photothermally induced gene expression in living cells and tissues by nanorod-locked nucleic acid complexes, Acs Nano 8 (4) (2014) 3597–3605.
[17] S. Wang, R. Riahi, N. Li, D.D. Zhang, P.K. Wong, Single cell nanobiosensors for dynamic gene expression profiling in native tissue microenvironments, Adv. Mater. 27 (39) (2015) 6034–6038.
[18] S. Wang, J. Sun, D.D. Zhang, P.K. Wong, A nanobiosensor for dynamic single cell analysis during microvascular self-organization, Nanoscale 8 (38) (2016) 16894–16901.
[19] R. Riahi, J. Sun, S. Wang, M. Long, D.D. Zhang, P.K. Wong, Notch1-Dll4 signalling and mechanical force regulate leader cell formation during collective cell migration, Nat. Commun. 6 (2015) 6556.
[20] S. Tao, S. Wang, S.J. Moghaddam, A. Ooi, E. Chapman, P.K. Wong, D.D. Zhang, Oncogenic KRAS confers chemoresistance by upregulating NRF2, Cancer Res. 74 (2014) 7430–7441.
[21] Z.B. Liu, S.S. Chen, B.W. Liu, J.P. Wu, Y.B. Zhou, L.Y. He, J.S. Ding, J.W. Liu, Intracellular detection of ATP using an aptamer beacon covalently linked to graphene oxide resisting nonspecific probe displacement, Anal. Chem. 86 (24) (2014) 12229–12235.
[22] D. Zheng, D.S. Seferos, D.A. Giljohann, P.C. Patel, C.A. Mirkin, Aptamer nanoflares for molecular detection in living cells, Nano Lett. 9 (9) (2009) 3258–3261.
[23] H. Cho, E.C. Yeh, R. Sinha, T.A. Laurence, J.P. Bearinger, L.P. Lee, Single-step nanoplasmonic VEGF165 aptasensor for early cancer diagnosis, Acs Nano 6 (9) (2012) 7607–7614.
[24] H. Kaur, L.Y. Yung, Probing high affinity sequences of DNA aptamer against VEGF165, PLoS One 7 (2) (2012) e31196.
[25] S. Zhang, H. Gao, G. Bao, Physical principles of nanoparticle cellular endocytosis, Acs Nano 9 (9) (2015) 8655–8671.
[26] Z.M. Bian, S.G. Elner, V.M. Elner, Thrombin-induced VEGF expression in human retinal pigment epithelial cells, Invest. Ophthalmol. Vis. Sci. 48 (6) (2007) 2738–2746.
[27] E. Dupuy, A. Habib, M. Lebret, R. Yang, S. Levy-Toledano, G. Tobelem, Thrombin induces angiogenesis and vascular endothelial growth factor expression in human endothelial cells: possible relevance to HIF-1alpha, J. Thromb. Haemostasis JTH 1 (5) (2003) 1096–1102.
[28] Z.S. Dean, R. Riahi, P.K. Wong, Spatiotemporal dynamics of microRNA during epithelial collective cell migration, Biomaterials 37 (2015) 156–163.
[29] R. Riahi, M. Long, Y. Yang, Z. Dean, D.D. Zhang, M.J. Slepian, P.K. Wong, Single cell gene expression analysis in injury-induced collective cell migration, Integr. Biol. Quant. Biosci. Nano Macro 6 (2) (2014) 192–202.
[30] Z.S. Dean, P. Elias, N. Jamilpour, U. Utzinger, P.K. Wong, Probing 3D collective cancer invasion using double-stranded locked nucleic acid biosensors, Anal. Chem. 88 (2016) 8902–8907.
[31] J. Sun, N. Jamilpour, F.Y. Wang, P.K. Wong, Geometric control of capillary architecture via cell-matrix mechanical interactions, Biomaterials 35 (10) (2014) 3273–3280.
[32] H. Parsa, R. Upadhyay, S.K. Sia, Uncovering the behaviors of individual cells within a multicellular microvascular community, P. Natl. Acad. Sci. U. S. A. 108 (12) (2011) 5133–5138.
[33] G. Serini, D. Ambrosi, E. Giraudo, A. Gamba, L. Preziosi, F. Bussolino, Modeling the early stages of vascular network assembly, Embo J. 22 (8) (2003) 1771–1779.
[34] G.C. Mo, B. Ross, F. Hertel, P. Manna, X. Yang, E. Greenwald, C. Booth, A.M. Plummer, B. Tenner, Z. Chen, Y. Wang, E.J. Kennedy, P.A. Cole, K.G. Fleming, A. Palmer, R. Jimenez, J. Xiao, P. Dedecker, J. Zhang, Genetically encoded biosensors for visualizing live-cell biochemical activity at super-resolution, Nat. Methods 14 (2017) 427–434.
[35] W. Risau, I. Flamme, Vasculogenesis, Annu. Rev. Cell Dev. Biol. 11 (1995) 73–91.
[36] R. Riahi, Z. Dean, T.H. Wu, M.A. Teitell, P.Y. Chiou, D.D. Zhang, P.K. Wong, Detection of mRNA in living cells by double-stranded locked nucleic acid probes, Analyst 138 (2013) 4777–4785.
[37] K. Sefah, D. Shangguan, X. Xiong, M.B. O'donoghue, W. Tan, Development of DNA aptamers using Cell-SELEX, Nat. Protoc. 5 (6) (2010) 1169–1185.
[38] E. Eden, N. Geva-Zatorsky, I. Issaeva, A. Cohen, E. Dekel, T. Danon, L. Cohen, A. Mayo, U. Alon, Proteome half-life dynamics in living human cells, Science 331 (6018) (2011) 764–768.
[39] T. Arcondeguy, E. Lacazette, S. Millevoi, H. Prats, C. Touriol, VEGF-A mRNA processing, stability and translation: a paradigm for intricate regulation of gene expression at the post-transcriptional level, Nucleic Acids Res. 41 (17) (2013) 7997–8010.
[40] J. Dibbens, D. Miller, A. Damert, W. Risau, M. Vadas, G. Goodall, Hypoxic regulation of vascular endothelial growth factor mRNA stability requires the cooperation of multiple RNA elements, Mol. Biol. Cell 10 (4) (1999) 907–919.